NUMERICAL MODELLING OF HIGH SPEED AND LOW SPEED COMBUSTION

RUPERT KLEIN (rupert.klein@zib.de)
FB Mathematik & Infomatik, Freie Universität Berlin

Abstract. The numerical simulation of turbulent combustion remains one of the most challenging problems of scientific computing. Major difficulties arise from a number of specific physical properties of combustion systems, which are extremely difficult to represent by discrete numerical approximations. This article explains three key problem areas that are relevant to premixed turbulent combustion and that are related to singular limit regimes of the underlying reactive flow equations. These problem areas are the low Mach number singularity, the deflagration and detonation discontinuity limits, and some issues arising from numerical integration of stiff and rapid chemical reaction equations. For each problem area we summarize the underlying physical processes and the relevant mathematical description, explain the associated numerical problems, and provide brief descriptions of numerical strategies to overcome them. This article is a condensation of two earlier extended reports by the author, published in Vervisch et al. (1999) and Breitung et al. (1999a).

Key words: turbulent premixed combustion, flame acceleration, low Mach number flow, stiff and rapid chemistry, numerical methods

1. Introduction

The conservation principles of mass, momentum, and energy in non-dimensional form may be written as

$$\begin{aligned}
&\frac{1}{\mathrm{Sr}}\,(\rho)_t \;+\; \nabla\cdot(\rho\boldsymbol{v}) &&= 0\\
&\frac{1}{\mathrm{Sr}}\,(\rho\boldsymbol{v})_t \;+\; \nabla\cdot\Big(\rho\boldsymbol{v}\circ\boldsymbol{v}+\frac{1}{M^2}\,\nabla p\Big)+\frac{1}{\mathrm{Re}}\,\nabla\cdot\boldsymbol{\tau} &&= 0\\
&\frac{1}{\mathrm{Sr}}\,(\rho e)_t \;+\; \nabla\cdot(\boldsymbol{v}[\rho e+p]) &&\\
&\qquad\qquad +\;\frac{1}{\mathrm{Re}}\nabla\cdot\left(\frac{1}{\mathrm{Pr}}\,\boldsymbol{j}_T+M^2\,\boldsymbol{\tau}\cdot\boldsymbol{v}+\frac{Q}{\mathrm{Sc}}\sum_{i=1}^{n_{\mathrm{spec}}}\delta h_i\,\boldsymbol{j}_i\right) &&= 0.
\end{aligned}\tag{1}$$

and the chemical species mass balances read as

$$\frac{1}{\mathrm{Sr}}\,(\rho Y_i)_t + \nabla\cdot(\rho Y_i \boldsymbol{v}) = -\frac{1}{\mathrm{ReSc}}\,\nabla\cdot\boldsymbol{j}_i + \mathrm{Da}\,\rho\omega_i \qquad (i = 1\ldots n_{\mathrm{spec}})\ . \quad (2)$$

Here $\rho, \boldsymbol{v}, p, e, \rho Y_i$ are the mass density, fluid flow velocity, pressure, total energy perunit mass, and the mass density of the ith species, respectively. The variables $\boldsymbol{\tau}, \boldsymbol{j}_T, \boldsymbol{j}_i$ denote the molecular transport of momentum, heat, and of the mass of the ith species, respectively.

The transport terms and the pressure are related to the mass, momentum, energy, and species densities through the caloric equation of state

$$\rho e \ = \ \frac{p}{\gamma - 1} + M^2\,\frac{1}{2}\rho\boldsymbol{v}^2 + Q\,\sum_{i=1}^{n_{\mathrm{spec}}} \Delta H_i\,\rho Y_i\ , \quad (3)$$

the thermal equation of state

$$T = \frac{p}{\rho}\,, \quad (4)$$

and the transport models

$$\begin{aligned} \boldsymbol{\tau} &= -\mu\left(\nabla\boldsymbol{v} + (\nabla\boldsymbol{v})^T\right) - \eta\,(\nabla\cdot\boldsymbol{v})\ \mathbf{1}\ , \\ \boldsymbol{j}_T &= -\kappa\nabla T\ , \qquad \boldsymbol{j}_i = -D_i\,\nabla Y_i\ . \end{aligned} \quad (5)$$

Notice that all physical quantities in these equations have been non-dimensionalized by (i.e., they are measured in units of) suitable reference quantities. The idea is that each non-dimensionalized quantity acquires values roughly of order unity, while the dimensionality of the physical quantity is carried by the non-dimensionalizing scaling factor. Thus, if a prime accent denotes a dimensional physical quantity, then the non-dimensional variables used above are defined as

$$\begin{aligned} \rho = \rho'/\rho'_{\mathrm{ref}}\ , \quad p = p'/p'_{\mathrm{ref}}\ , \quad \boldsymbol{v} = \boldsymbol{v}'/u'_{\mathrm{ref}}\ , \\ T = T'/(p'_{\mathrm{ref}}/(\rho'_{\mathrm{ref}}R'_{\mathrm{ref}}))\ , \quad e = e'/(p'_{\mathrm{ref}}/\rho'_{\mathrm{ref}})\ , \end{aligned} \quad (6)$$

and

$$\boldsymbol{x} = \boldsymbol{x}'/\ell'_{\mathrm{ref}}, \quad t = t'/t'_{\mathrm{ref}}\,. \quad (7)$$

In equations (1) and (3) we have introduced the scaled reaction enthalpies $\Delta H_i = \Delta H'_i/\Delta H'_{\mathrm{ref}}$ and the transport coefficients $\mu = \mu'/\mu'_{\mathrm{ref}}, \kappa = \kappa'/\kappa'_{\mathrm{ref}}$.

The procedure of scaling the equations has led to a set of seven characteristic numbers:

Abbreviation	**Definition**	**Name**
Sr	$t_{\rm ref} u_{\rm ref}/\ell_{\rm ref}$	Strouhal number
M	$u_{\rm ref}/\sqrt{p_{\rm ref}/\rho_{\rm ref}}$	Mach number
Re	$\rho_{\rm ref} u_{\rm ref} \ell_{\rm ref}/\mu_{\rm ref}$	Reynolds number
Pr	$\mu_{\rm ref}/(\kappa_{\rm ref}/R_{\rm ref})$	Prandtl number
Sc	$\mu_{\rm ref}/\rho_{\rm ref} D_{\rm ref}$	Schmidt number
Da	$\omega_{\rm ref}\ell_{\rm ref}/u_{\rm ref}$	Damköhler number
Q	$(\Delta H)_{\rm ref}/(p_{\rm ref}/\rho_{\rm ref})$	Heat Release Parameter

(8)

The exercise of non-dimensionalization and scaling induces the following observations:

1. *The low Mach number singularity.* As the Mach number M vanishes, the pressure gradient term in the momentum equation becomes singular. The low Mach number limit is very important in combustion because most technical combustion systems operate in this regime. Even for explosions the regime is relevant during the initial phase of flame acceleration.
2. *The detonation limit.* For large Damköhler numbers Da $\gg 1$ there is another singular limit that is very important for combustion applications. Detonations are propagating reactive discontinuities moving at very high speeds, much larger in fact, than the speed of sound in the unburnt gas mixture. These fronts propagate through purely gasdynamic chemical interactions in which molecular transport is unimportant. Their correct numerical representation, too, is very subtle.
3. *The deflagration limit.* A distinguished limit of large Damköhler numbers Da $\gg 1$ and inefficient molecular transport Re $\gg 1$ reveals the mathematical structure of laminar deflagrations (see (Teng et al., 1982; Matalon and Matkowsky, 1982; Majda and Sethian, 1985)). In the limit, these are propagating reactive discontinuities whose correct numerical representation is extremely subtle.
4. *Stiff and fast chemistry singularities.* Some chemical reactions involving chemical radicals do not considerably contribute to the net chemical energy conversion but nevertheless play an important role. These reactions typically feature large Damköhler numbers. Numerical challenges arise because minute concentrations of extremely reactive species must be computed on the basis of governing equations with extremely large rates. This leads to the typical numerical problem of "cancellation of significant digits" in finite computer arithmetics.

Each Section in this article will focus on one of these aspects and will introduce some basic concepts needed to follow the subsequent explanations concerning the structure of appropriate numerical methods.

Thus Section 2 gives an account of the some popular finite-difference and finite-volume numerical methods for low Mach number reactive flows.

Section 3 prepares the theoretical ground for the subsequent material by discussing some mathematical features of premixed combustion fronts. In particular, a discussion of the Rankine-Hugoniot jump conditions for gasdynamic discontinuities will be combined with a characteristic analysis of the (nearly-inviscid) flow of burnt and unburnt gases. This combination allows us to draw a number of conclusions regarding those features of the different types of fronts that are relevant for their numerical representation.

Section 4 concentrates on the problem of "fake numerical weak detonations" that are observed in under-resolved numerical simulations of high-speed combustion fronts. It will be explained why detonations—in contrast to reasonable expectations—cannot be easily captured in the same way as non-reacting shocks waves. A simple, practical resolution of these issues will be explained that relies on a judicious modification of the reaction kinetics. Notably, this modification does not affect the structure of a detonation when it can be resolved in detail, but it removes the "fake waves" when it cannot.

Sections 5 will address the numerical challenges in representing deflagration fronts. In constructing appropriate schemes one must decide whether (i) to include detailed models of all relevant physical processes within the turbulent combustion region or (ii) to consider the reaction front as a surface of discontinuity embedded between the burnt and unburnt gas regions. The former ansatz requires higher numerical resolution and more sophisticated and detailled modelling; the latter compromises on details but provides better control of what is and what is not modelled, because it restricts modelling to a few well-defined submodules. Some pro's and con's of these alternatives will be discussed.

The last issue of stiff chemistry will not be addressed in this paper due to lack of space and in favour of presenting a more detailed discussion of the previous items. The reader is referred to Warnatz et al. (1996), Peters (2000), Klein (1999) for comprehensive overviews.

Section 6 will provide a brief summary of the physical mechanism that are thought to be responsible for the so-called "Deflagration-to-Detonation-Transition (DDT)". From that section it will become clear that successful numerical prediction tools for fire and explosion safety will have to face all of the challenges discussed above, and they will thus have to incorporate a large number of sophisticated numerical technologies.

Section 7 provides a summary and a number of conclusions.

2. Low Mach Number Reactive Flows

In most real-life applications combustion-driven velocities are very small compared with the speed of sound. This has profound consequences for the numerical solution of the governing equations. In the limit, the elasticity of the gas with respect to inertial forces becomes negligible and soundwave propagation unnoticeable. Mathematically, this is a consequence of the singularity of the pressure gradient term as the Mach number M from (8) tends to zero. A formal asymptotic analysis, closely following Majda and Sethian (1985), Klein (1995) and Schneider et al. (1999), allows us to explore the consequences of this singularity.

2.1. ASYMPTOTIC ANALYSIS

For simplicity we consider an ideal gas mixture with a single-step reaction. Under these conditions we need to describe the time evolution of only the fuel mass fraction Y_F using a single transport equation of the type described in (2). The asymptotic solution ansatz

$$\begin{aligned} p &= p_0(\boldsymbol{x},t) + Mp_1(\boldsymbol{x},t) + M^2p_2(\boldsymbol{x},t) + o(M^2), \\ \boldsymbol{v} &= \boldsymbol{v}_0(\boldsymbol{x},t) + M\boldsymbol{v}_1(\boldsymbol{x},t) + o(M), \\ \rho &= \rho_0(\boldsymbol{x},t) + M\rho_1(\boldsymbol{x},t) + o(M), \\ Y_F &= Y_{F,0}(\boldsymbol{x},t) + MY_{F,1}(\boldsymbol{x},t) + o(M) \end{aligned} \tag{9}$$

is introduced into the dimensionless governing equations (1), (2). Following standard procedures of asymptotic analysis, one obtains a hierarchy of equations for the various expansion functions $p_i, \boldsymbol{v}_i, \rho_i, Y_{F,i}$. The momentum equations to orders M^{-2} und M^{-1} become

$$\nabla p_0(\boldsymbol{x},t) = 0\,, \quad \nabla p_1(\boldsymbol{x},t) = 0\,. \tag{10}$$

One concludes that p_0 and p_1 depend on time only in this regime of length and time scales, so that

$$p_0 \equiv P_0(t) \qquad \text{and} \qquad p_1 \equiv P_1(t)\,. \tag{11}$$

The continuity and energy equations at leading order are then

$$\frac{\partial \rho_0}{\partial t} + \nabla\cdot(\rho_0\boldsymbol{v}_0) = 0 \tag{12}$$

$$\frac{1}{\gamma-1}\frac{dP_0}{dt} + \nabla\cdot(H_0\boldsymbol{v}_0) = \Big(\frac{1}{\mathrm{Pe}}\nabla\cdot(\lambda\nabla T_0) + \mathrm{Da}\,Q\,\rho\omega_F\Big)\,, \tag{13}$$

where

$$H_0(t) = \frac{\gamma}{\gamma - 1} P_0(t) \,. \tag{14}$$

Equation (13) is a consequence of the expansion (9) used in $(1)_3$, and the gradient condition from (10). The momentum equation at order M^0 reads

$$\frac{\partial \rho_0 \boldsymbol{v}_0}{\partial t} + \nabla\cdot (\rho_0 \boldsymbol{v}_0 \circ \boldsymbol{v}_0) + \nabla p_2 = -\frac{1}{\mathrm{Re}} \nabla\cdot\boldsymbol{\tau}_0 \,. \tag{15}$$

Notice the change in structure of these equations: The pressure evolution equation does *not* determine the pressure variable p_2 appearing in the momentum equation! The appropriate interpretation, corresponding directly to the theory of incompressible flows, is that the equation for P_0 from (13) is a divergence constraint for the leading order energy flux, and that the second order pressure p_2 is responsible for guaranteeing that constraint to be observed. In fact, (13) may be recast as a

$$\nabla\cdot\boldsymbol{v}_0 = -\frac{1}{\gamma P_0} \left[\frac{dP_0}{dt} - (\gamma - 1)\Big(\frac{1}{\mathrm{Pe}} \nabla\cdot (\lambda \nabla T_0) + \mathrm{Da}\, Q \rho \omega_F \Big) \right] . \tag{16}$$

which is obtained by using that $H_0(t) = \gamma P_0(t)/(\gamma - 1)$ is a function of time only. Thus chemical heat release, heat conduction, and global pressure changes conspire to induce a divergence field for the velocity.

Mass continuity (12) now provides an equation for the evolution of the density along particle paths

$$\frac{D\rho}{Dt} := \frac{\partial \rho}{\partial t} + \boldsymbol{v} \cdot \nabla \rho = -\rho \nabla\cdot \boldsymbol{v} \,. \tag{17}$$

The original interpretation of (16) as an energy flux divergence constraint proves to be useful in the construction of energy-conserving finite-volume methods, see (Schneider et al., 1999; Klein, 1999).

Equations (12) to (15) form a closed system, provided the temporal evolution of the leading-order pressure P_0 is known and the state dependence of the reaction rate $\rho\omega_F$ is given. For combustion under atmospheric conditions P_0 equals the atmospheric ambient pressure and is constant in time. For combustion in a closed chamber, we explore the fact that P_0 is homogeneous in space, integrate (16) over the total flow domain, and obtain

$$\frac{dP_0}{dt} = \frac{1}{\Omega} \left[- \oint_{\partial V} \left(\gamma P_0 \boldsymbol{v} - \frac{\gamma - 1}{\mathrm{Pe}} \lambda \nabla T_0 \right) \cdot \boldsymbol{n} \, d\sigma + \mathrm{Da} \int_V (\gamma - 1) Q \rho \omega_F \, dV \right] . \tag{18}$$

Here $\boldsymbol{n}$ is the outward pointing unit normal at the boundary, and $\Omega = \int_V dV$ is the total volume of the domain of integration V. Given velocity and thermal boundary conditions all changes of the background pressure are thus related to the overall chemical energy conversion within the domain.

With respect to the divergence constraint, the structure of the above equations is similar to that of incompressible, non-reactive flow. Appropriate extensions of incompressible flow solvers should be able to handle zero Mach number reactive flows as well. The reader may want to consult Fletcher (1988), Issa (1986), Kim and Moin (1985), and Patankar (1980) for reviews of typical developments based on this approach. Further aspects of low Mach number asymptotics, including the influence of high-frequency and long-wavelength acoustic perturbations, are discussed in Klein and Peters (1988), and Klein (1995).

2.2. NUMERICAL CONSEQUENCES OF THE ASYMPTOTICS

The most important consequence of the asymptotics is the pressure decomposition. Both the leading-order spatially homogeneous part $P_0(t)$ and the $O(M^2)$-perturbation $p_2(\boldsymbol{x}, t)$ enter the leading-order system of equations through (16) and (15). This splitting of the pressure is essential because a numerical method designed to integrate the original compressible flow equations must *necessarily* fail when applied to very low Mach number combustion problems, unless special care is taken to introduce an appropriate separation and re-scaling of the pressure mean and its fluctuations.

Consider a smooth low Mach number flow on a domain of characteristic size ℓ. The total pressure variation within the flow domain will be $M^2\,\delta p_2$, where $\delta p_2 = O(1)$ as $M \to 0$. Assume that the flow domain is discretized by n grid points across the length of ℓ so that the grid spacing is $\Delta x = \ell/n$. A second-order discrete representation of the derivative $\partial p/\partial x$ on a carthesian grid with constant spacing in the x-direction would read

$$\frac{\partial\, p}{\partial x} = \frac{p_{i+1,j} - p_{i-1,j}}{2\Delta x} + O((\Delta x)^2)\,. \tag{19}$$

In the low Mach number limit, the pressure in the vicinity of the centre cell i can be expressed as

$$p(x) = p_i + M^2(x - x_i)\frac{\partial p_2}{\partial x} + O(M^2(\Delta x)^2)\ . \tag{20}$$

In a typical situation the pressures p_{i-1}, p_{i+1} would thus scale as

$$\begin{aligned} p_{i-1} &= p_i - M^2\,\Delta x\ p_2'\,, \\ p_{i+1} &= p_i + M^2\,\Delta x\ p_2'\,, \end{aligned} \qquad \big(p_2' = O(1) \quad \text{as} \quad M, \Delta x \to 0\big)\,. \tag{21}$$

Now let, e.g., $p_i = 1.0$, $p_2' = 1.0$ and insert the exact results from this equation into the discrete differentiation formula from (19). Evaluating the discrete gradient using a sequence of Mach numbers $M = 10^{-2}...10^{-4}$

and resolutions $\Delta x = 10^{-1}...10^{-3}$ we obtain the numerical round-off errors and truncation error estimates $(\Delta x)^2$ for both single- and double-precision arithmetics in Table I. We conclude:

1. Single precision computations will fail already at $M = 10^{-2}$.
2. Double precision evaluations begin to deteriorate for $M < 10^{-3}$.
3. In contrast to intuition, increasing numerical resolution will *worsen* the problem rather than alleviating it!

Table I. Round-off versus truncation errors for a single evaluation of $\partial p/\partial x$

$\Delta x/\ell$	M	$\frac{p_{i+1}-p_{i-1}}{2M^2\Delta x}$	$\frac{\text{err}_{\text{single}}}{(\Delta x)^2}$	$\frac{\text{err}_{\text{double}}}{(\Delta x)^2}$
0.1	10^{-2}	1.111	$2.12 \cdot 10^{-1}$	$1.72 \cdot 10^{-10}$
	10^{-3}	$''$	7.29	$7.98 \cdot 10^{-8}$
	10^{-4}	$''$	$1.0 \cdot 10^{2}$	$3.72 \cdot 10^{-6}$
0.01	10^{-2}	1.111	$7.23 \cdot 10^{2}$	$1.72 \cdot 10^{-8}$
	10^{-3}	$''$	$1.0 \cdot 10^{4}$	$2.80 \cdot 10^{-5}$
	10^{-4}	$''$	$1.0 \cdot 10^{4}$	$1.63 \cdot 10^{-3}$
0.001	10^{-2}	1.111	$7.29 \cdot 10^{4}$	$7.98 \cdot 10^{-4}$
	10^{-3}	$''$	$1.0 \cdot 10^{6}$	$3.72 \cdot 10^{-2}$
	10^{-4}	$''$	$1.0 \cdot 10^{6}$	0.16

For further reading on the round-off error problem for low Mach number computations see (Sesterhenn et al., 1992).

We conclude that a numerical scheme that does not take into account the order-of-magnitude decomposition of the pressure field into, at least, a leading order thermodynamic term, P_0, and a second order term $M^2 p_2$ will not be able to represent very slow flows. The next subsection describes the popular strategy of "projection methods", which explicitly introduce such a decomposition and solve appropriate limit equations to obtain the second order pressure field. Notice that more elaborate "Multiple Pressure Variable (MPV)" schemes have been suggested in (Klein, 1995; Geratz et al., 1996; Roller et al., 1999; Schneider et al., 1999), which even account for leading

order acoustic effects on the velocity field and which, accordingly, include a term Mp_1 in the pressure decomposition.

2.3. PROJECTION-TYPE METHODS FOR LOW MACH NUMBER FLOWS

Here we summarize briefly the concept of Projection-type methods for low Mach number flows, which borrow from (Chorin, 1967; Chorin, 1968; Chorin, 1969). The alternative SIMPLE-type schemes, (Patankar, 1980; Karki and Patankar, 1989; Rhie, 1989; Shyy, 1994; Haldenwang et al., 1998; Geratz et al., 1996; Roller et al., 1999), and Finite-element methods, (Rannacher, 1992; Hughes, 1995; Löhner et al., 1997; Lang, 1998), will not be addressed in this section owing to lack of space and the author's personal experience in using these.

The key idea of projection schemes can best be described by considering constant density incompressible inviscid flows. The governing equations are obtained from those derived in Section 2.1 by assuming zero heat release, $Q \equiv 0$, and constant density, $\rho \equiv 1$, by passing to the limit of infinite Reynolds and Peclet numbers, $(\mathrm{Re}, \mathrm{Pe} \rightarrow \infty)$ and then considering the zero Mach number limit, $M \equiv 0$. The continuity equation in that case becomes redundant, the momentum equation reduces to

$$\frac{\partial \boldsymbol{v}}{\partial t} + \boldsymbol{v} \cdot \nabla \boldsymbol{v} + \nabla p_2 = 0 \ , \tag{22}$$

and the leading-order energy equation yields the homogeneous velocity divergence constraint

$$\nabla \cdot \boldsymbol{v} = 0 \ . \tag{23}$$

Notice that $\nabla \cdot (\boldsymbol{v} \circ \boldsymbol{v}) \equiv \boldsymbol{v} \cdot \nabla \boldsymbol{v}$ when $\nabla \cdot \boldsymbol{v} \equiv 0$!

A projection scheme consists of 2 steps. Step 1 accounts for non-linear convection, $\boldsymbol{v} \cdot \nabla \boldsymbol{v}$, in an explicit fashion by solving the truncated system

$$\frac{\partial \boldsymbol{v}}{\partial t} + \boldsymbol{v} \cdot \nabla \boldsymbol{v} = 0 \tag{24}$$

over one time step. Given the velocity field $\boldsymbol{v}^n$ at time t^n, the first step provides a mapping

$$\boldsymbol{v}^* = \boldsymbol{v}^n - \Delta t \ (\boldsymbol{v} \cdot \nabla \boldsymbol{v})^n \tag{25}$$

with a suitable numerical approximation of the convection terms. There is no guarantee that $\boldsymbol{v}^*$ will satisfy the divergence condition from (23), and so the second step consists of "projecting" this intermediate velocity field back onto the space of divergence-free fields:

$$\boldsymbol{v}^{n+1} = \boldsymbol{v}^* - \nabla \phi \, , \tag{26}$$

with ϕ adjusted so as to let $\boldsymbol{v}^{n+1}$ comply with the divergence constraint, i.e.,

$$\nabla^2\phi = \nabla\cdot\boldsymbol{v}^* \,. \tag{27}$$

That the correction to $\boldsymbol{v}^*$ should be in the form of a gradient field becomes intuitively clear from a comparison of the original momentum (22) and the truncated one from the first projection step (24). It was the pressure gradient field that was left out in formulating the first step of the scheme. More elaborate explanations and justifications, based on the general Helmholtz-Hodge decomposition of vector fields, are given in the original references (Chorin, 1967; Chorin, 1968; Chorin, 1969) and in related subsequent publications (Bell and Marcus, 1992; Lai et al., 1993; van Kan, 1986; Gresho et al., 1991; Almgren et al., 1996). The reader may also want to consult Rannacher (1992) for detailed discussions of some difficulties and pitfalls associated with this approach.

Major efforts have recently been spent to extend this approach by introducing higher-order approximations, dynamic adaptive grid refinement (Berger and Colella, 1989), and by allowing variable densities (while still keeping the zero divergence constraint!), (Bell and Marcus, 1992; Almgren et al., 1996). Further extensions aim at the representation of low Mach number reacting flows (Lai et al., 1993; Pember et al., 1996).

2.4. THE INFLUENCE OF LONG WAVELENGTH ACOUSTICS

The construction of an asymptotic solution ansatz as in (9) requires some hypotheses regarding the nature of the solution. In many applications one is interested in the interaction of acoustic waves and combustion processes. For example, the excitation of acoustic waves by unsteasy combustion can lead to unacceptable noise levels of technical combustion devices, and acoustic-combustion resonances may even endanger their integrity. A key feature of systems in which acoustic-combustion resonances occur is that the characteristic time scales of convection, reaction progress, and acoustic oscillations are comparable. At a first glance this seems to imply that the flow must be fully compressible, because "common sense" has it that acoustics would always be of "high frequency" as long as the flow Mach numbers are small. This, however, is not correct.

Suppose that an oscillating flame, burning at a characteristic flame speed of about 1 m/s generates acoustic waves. Obviously, because the flame is the sole source of acoustics in this case, the pressure waves inherit the flame's oscillation time scale. The difference in propatation speeds between acoustics pulses on the one hand, and the flame and the convective gas flow on the other in this case manifests itself through a difference in the characteristic lengths of the associated phenomena rather than in their

time scales. Figure 1 elucidates this point. Figure 1a shows a characteristic diagram for a situation in which uncorrelated pressure, density and velocity perturbations of a common characteristic wavelength are imposed at some initial time. These perturbations decompose into acoustic and convective phenomena, thereby leading to a clear time scale separation. In contrast, Figure 1b shows the situation when all perturbations are generated in time by the same source, such as an oscillating flame. In this case, the characteristic diagram reveals a multiple *space* scale regime rather than multiple time scales.

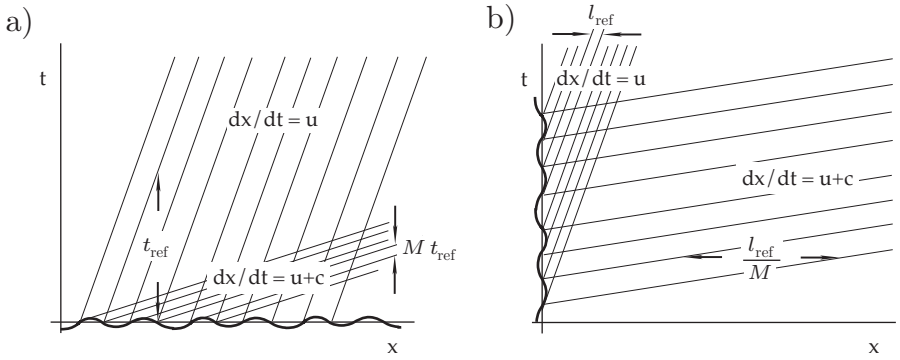

Figure 1. Two distinct low Mach number flow regimes: a) single time scale – multiple space scales (long wave acoustics), b) multiple time scales – single space scale (high frequency acoustics).

An asymptotic solution ansatz designed to capture this single time scale—multiple length scale regime has been proposed by Klein (1995). The pressure expansion scheme, which is representative for the expansion of all flow variables, reads as

$$p = p_0(\boldsymbol{x}, \boldsymbol{\xi}, t) + Mp_1(\boldsymbol{x}, \boldsymbol{\xi}, t) + M^2 p_2(\boldsymbol{x}, \boldsymbol{\xi}, t) + o(M^2), \tag{28}$$

where the additional space coordinate

$$\boldsymbol{\xi} \equiv M\boldsymbol{x}, \tag{29}$$

resolves long wavelength acoustic phenomena.

Klein (1995) applies standard procedures of multiple scales asymptotics to derive the first closed set of asymptotic limit equations. The momentum equations at orders M^{-2} and M^{-1} yield

$$\nabla_{\boldsymbol{x}} p_0 = \nabla_{\boldsymbol{\xi}} p_0 = \nabla_{\boldsymbol{x}} p_1 \equiv 0\ , \tag{30}$$

so that

$$p_0 \equiv P_0(t) \qquad \text{and} \qquad p_1 \equiv P_1(\boldsymbol{\xi}, t)\ . \tag{31}$$

Next the mass, momentum, and energy balances at order M^0 are

$$\begin{aligned} \frac{\partial \rho}{\partial t} &+ \nabla_{\boldsymbol{x}}\cdot(\rho \boldsymbol{v}) &&= 0 \\ \frac{\partial \rho \boldsymbol{v}}{\partial t} &+ \nabla_{\boldsymbol{x}}\cdot(\rho \boldsymbol{v}\circ\boldsymbol{v}) + \nabla_{\boldsymbol{x}} p_2 &&= -\nabla_{\boldsymbol{\xi}} P_1 \\ \frac{dP_0}{dt} &+ \gamma P_0(t)\nabla_{\boldsymbol{x}}\cdot\boldsymbol{v} &&= 0\,. \end{aligned} \tag{32}$$

The $\boldsymbol{x}$-average of this equation yields

$$\frac{dP_0}{dt} \equiv 0 \qquad \text{or} \qquad \nabla_{\boldsymbol{x}}\cdot\boldsymbol{v} \equiv 0\,. \tag{33}$$

Finally, the $\boldsymbol{x}$-averaged mass balance and momentum equation at order M^0 and energy equation at order M^1 provide a set equations describing the time evolution of the system on the large "acoustic" scales

$$\begin{aligned} \frac{\partial \overline{\rho}}{\partial t} &&&= 0 \\ \frac{\partial \overline{\rho \boldsymbol{v}}}{\partial t} &+ \nabla_{\boldsymbol{\xi}} P_1 &&= 0 \\ \frac{\partial P_1}{\partial t} &+ \nabla_{\boldsymbol{\xi}}\cdot(\gamma P_0 \overline{\boldsymbol{v}}) &&= 0\,. \end{aligned} \tag{34}$$

Equations (31) – (34) describe the evolution of the leading order velocity and density fields and of the leading, first and second order pressure fields. They form the first closed set of equations that is obtained from the multiple scales asymptotic expansion from (28).

In absence of long wavelength effects, $(\partial/\partial\boldsymbol{\xi} \equiv 0)$, the small scale equations (34) and (35) reduce to the equations for incompressible, variable density flow. In the presence of long wave effects, but for density distributions that do not, at leading order, depend on the short scale variable $\boldsymbol{x}$, one has $\overline{\rho\boldsymbol{v}} \equiv \rho\overline{\boldsymbol{v}}$ and the long wave equations (34) are equivalent to linear acoustics. If, however, there is small scale variation of both density ρ and velocity $\boldsymbol{v}$, then the relation

$$\overline{\boldsymbol{v}} = \frac{1}{\overline{\rho}}(\overline{\rho\boldsymbol{v}} - \overline{\tilde{\rho}\tilde{\boldsymbol{v}}}) \tag{35}$$

and (34) may be rewritten as

$$\begin{aligned} \frac{\partial \overline{\rho}}{\partial t} &&&= 0 \\ \frac{\partial \overline{\rho \boldsymbol{v}}}{\partial t} &+ \nabla_{\boldsymbol{\xi}} P_1 &&= 0 \\ \frac{\partial P_1}{\partial t} &+ \nabla_{\boldsymbol{\xi}}\cdot(c^2\ \overline{\rho\boldsymbol{v}}) &&= \nabla_{\boldsymbol{\xi}}\cdot(c^2\ \overline{\tilde{\rho}\tilde{\boldsymbol{v}}})\,. \end{aligned} \tag{36}$$

Here $c^2 = \gamma P_0/\overline{\rho}$. This version of the large scale equations reveals that there is a non-trivial interaction between long wavelength linear acoustics in terms of the variables $P_1(\boldsymbol{\xi}, t)$ and $\overline{\rho \boldsymbol{v}}$ and the correlation of small scale density and velocity fluctuations through the energy flux contribution $c^2\ \overline{\tilde{\rho}\tilde{\boldsymbol{v}}}$.

That this interaction goes both ways becomes clear upon close consideration of the small scale momentum equation $(32)_2$. Suppose that two neighboring mass elements with leading order densities ρ_1 and ρ_2 are accelerated by a common large scale acoustic pressure gradient, represented by $\nabla_{\boldsymbol{\xi}} P_1$. As the *momentum change* of both mass elements is the same (see the equation), there velocities must necessarily differ by a factor of ρ_2/ρ_1. As a consequence of this differential acceleration vorticity is generated. This so-called "baroclinic effect" and the previously mentioned source term in the long wave acoustic equations, $\nabla_{\boldsymbol{\xi}} \cdot (c^2\ \overline{\tilde{\rho}\tilde{\boldsymbol{v}}})$, lead to a mutual interaction between the small-scale, quasi-incompressible and the large-scale acoustic flows.

As an example that elucidates the effect we consider a right-running acoustic wave that passes over a saw-tooth like density profile which is thereby set into motion. The mechanism of baroclinic vorticity generation leads to the establishment of a vortex sheet, which subsequently undergoes a Kelvin-Helmholtz instability. The initially horizontal interface starts rolling up into a hierarchy of vortical structures as shown in Fig. 2. These results have been obtained by initializing a flow simulation in a double-periodic domain

$$\begin{array}{rcccl} -L & \leq x \leq & L & = & \frac{1}{M} \\ 0 & \leq y \leq & L_y & = & \frac{2L}{5} \end{array}; \quad M = \frac{1}{20}, \tag{37}$$

which was discretized by 400×80 grid cells. The initial data

$$\begin{array}{lcl} \rho(x,y,0) & = & 1.0 \quad + \ 0.2M(1.0 + cos(\pi x/L)) \ + \Phi(y), \\ p(x,y,0) & = & 1.0 \quad + \ \ M\gamma(1.0 + cos(\pi x/L)), \\ u(x,y,0) & = & \sqrt{\gamma}(1.0 + cos(\pi x/L)), \\ v(x,y,0) & = & 0.0, \end{array} \tag{38}$$

With $\rho_y = 0.8/L_y$, the function $\Phi(y)$ is defined by

$$\Phi(y) = \begin{cases} \rho_y y & \text{for} \quad 0 \leq y \leq \frac{1}{2}L_y, \\ \rho_y(y - \frac{1}{2}L_y) - 0.4 & \text{for} \ \frac{1}{2}L_y < y \leq L_y. \end{cases} \tag{39}$$

These initial data represent a saw-tooth like density layering in the y-direction. In x-direction, a right-running, long wavelength acoustic pulse is superimposed, which subsequently sets the density layering in motion. As explained above, vorticity is generated due to the transverse density variation. A sharp shear discontinuity appears in the vicinity of the density jump. As time procedes, the shear layer develops a Kelvin-Helmholtz

instability which saturates into large scale coherent vortices. These and

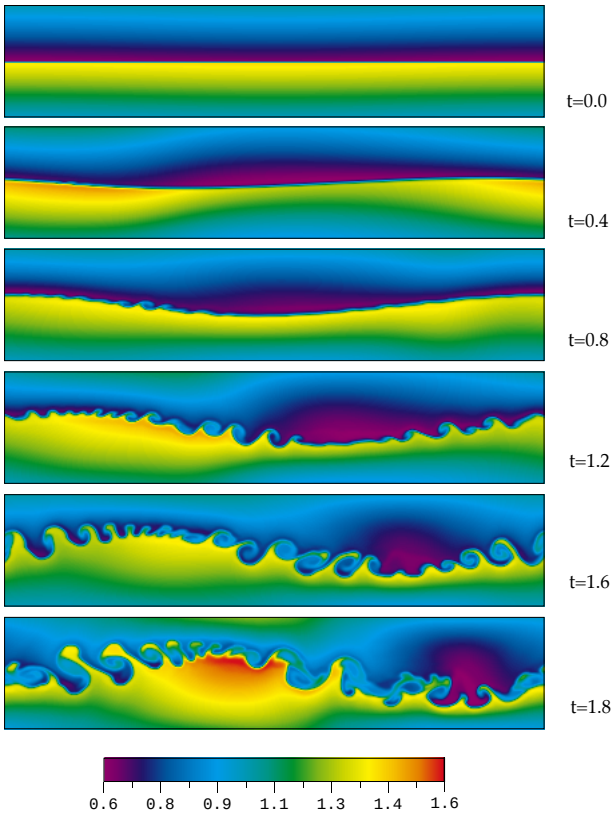

Figure 2. Temporal evolution of density layering under an acoustic pulse

similar simulations have been described in (Geratz, 1998; Geratz et al., 1996; Roller et al., 1999). In these publications, a family of low Mach number flow solvers has been introduced that makes explicit use of the asymptotics described originally by Klein (1995) and summarized earlier in this section.

The idea in constructing these numerical methods is to extend a scheme that is able to handle variable density incompressible flows by a large time step predictor that efficiently incorporates the influence of long wavelength acoustics. In the spirit of a classical projection method, (Chorin, 1968; Chorin, 1969), one first generates explicit estimates of the influence of advection / convection on the flow field (the terms involving the transport operator $\boldsymbol{v} \cdot \nabla\{\cdot\}$ or its conservative form $\nabla\cdot(\rho\boldsymbol{v}\,\{\cdot\})$). Next, the long wave acoustic equations (34) are solved over one time step on the basis of long wave filtered initial data. The latter are extracted from the current flow field

by applying suitable low pass filter techniques. The obtained increments of the flow variables are added to the previous convective predictions, before the time step is completed by applying the final "projection step". In the case of zero Mach number incompressible flow, this projection step guarantees that the flow field is discretely divergence-free after completion of the time step. In the case of weakly compressible flows, the asymptotics suggests that the energy equation be used to formulate the projection step. (Note that the small scale divergence constraint, $\nabla_{\boldsymbol{x}} \cdot \boldsymbol{v} \equiv 0$, from (35) is a result of the leading order energy equation!) For more details the reader is referred to the publications cited above and, in addition, to some closely related work in (Knio and Worlikar, 1996; Knio et al., 1998; Knio et al., 1999; Schneider et al., 1999).

Such interactions between long wave acoustics and steep density gradients are extremely important for premixed combustion processes. Sharp density variations as displayed in the above test case are one of the major characteristics of deflagration waves in realistic systems. If combustion can resonate with acoustic modes of a container or combustion chamber, the baroclinic vorticity generation just explained may dramatically enhance the net combustion rates through intense flame stretching and the subsequent rapid increase of the effective flame area. This mechanism of acoustics-induced flame acceleration is listed by Breitung et al. (1999a) as one prominent player in Deflagration-to-Detonation Transition Processes (see also section 6).

3. Mathematics of deflagrations and other discontinuities

For simplicity, we restrict much of the discussion of this section to a single space dimension. The key observations will not depend on this limitation.

3.1. JUMP CONDITIONS

Consider one-dimensional travelling wave solutions in an unbounded domain of the scaled governing equations from Equations (1) to (7). Any variable $\phi(\boldsymbol{x}, t)$ would be described by

$$\phi(\boldsymbol{x}, t) = \tilde{\phi}(x - Dt)\,, \tag{40}$$

where it is assumed that the wave travels in the x-direction at velocity D. Inserting this ansatz in the governing equations we obtain

$$\begin{aligned}
-D\frac{d}{d\xi}(\rho) \;+\; \frac{d}{d\xi}(\rho u) \qquad\qquad &= \;0 \\
-D\frac{d}{d\xi}(\rho u) \;+\; \frac{d}{d\xi}(\rho u^2 + \frac{1}{M^2}\,p) \;&=\; -\frac{d}{d\xi}\left(\frac{1}{\mathrm{Re}}\tau_{x,x}\right) \\
-D\frac{d}{d\xi}(\rho e) \;+\; \frac{d}{d\xi}(u[\rho e + p]) \qquad &= \\
-\frac{d}{d\xi}\left(\frac{1}{\mathrm{Pe}}j_{T,x} + \frac{M^2}{\mathrm{Re}}\tau_{x,x}u + \frac{Q}{\mathrm{ReSc}}\sum_{i=1}^{n_{\mathrm{spec}}}\Delta H_i\, j_{i,x}\right)&.
\end{aligned} \tag{41}$$

from the conservation laws and

$$-D\frac{d}{d\xi}(\rho Y_i) + \frac{d}{d\xi}(\rho Y_i u) = -\frac{d}{d\xi}\left(\frac{1}{\mathrm{ReSc}}\,j_{i,x}\right) + \mathrm{Da}\rho\omega_i\,, \tag{42}$$

for $(i = 1 \ldots n_{\mathrm{spec}})$, from the species balances. Here $\xi = x - Dt$ and $\tau_{x,x}, j_{T,x}, j_{i,x}$ are the x-components of the x-stress component, the heat conduction energy flux and the ith species diffusion fluxes, respectively.

Next, we integrate in ξ assuming that constant burnt and unburnt gas conditions $(\rho, u, p, Y_i)_b$ and $(\rho, u, p, Y_i)_u$ are attained as $\xi \to -\infty$ and $\xi \to \infty$, respectively. Under these assumptions, the diffusive fluxes and the heat conduction terms vanish as $|\xi| \to \infty$ because they are proportional to gradients of the dependent variables. Integration of (41) yields

$$\begin{aligned}
-D[\![\rho]\!] \;+\; [\![\rho u]\!] \qquad\qquad &= \;0 \\
-D[\![\rho u]\!] \;+\; [\![\rho u^2 + \tfrac{1}{M^2}\,p]\!] \;&=\; 0 \\
-D[\![\rho e]\!] \;+\; [\![u(\rho e + p)]\!] \;&=\; 0.
\end{aligned} \tag{43}$$

These are the standard Rankine-Hugoniot jump condtions for gas dynamic discontinuities.

Since we assume that at large distances two constant states of burnt and unburnt should be attained, we must require that the chemical reaction rates vanish at both ends:

$$\boldsymbol{\omega}(T_u, p_u, \boldsymbol{Y}_u) = \boldsymbol{\omega}(T_b, p_b, \boldsymbol{Y}_b) = 0 \tag{44}$$

where

$$\boldsymbol{Y} = \{Y_j\}_{j=1}^{n_{\mathrm{spec}}} \qquad \text{and} \qquad \boldsymbol{\omega} = \{\omega_j\}_{j=1}^{n_{\mathrm{spec}}}\,. \tag{45}$$

In the unburnt gas this constraint is normally satisfied automatically because the reactions are frozen at low temperatures. Therefore, as in real-life

applications, the unburnt gas composition can be chosen more or less arbitrarily. For the burnt gas one obtains a non-trivial constraint because temperatures will generally be high enough to allow chemical reactions to be active. Thus one may read the second equality in (44) as algebraic constraints for the equilibrium species mass fractions $\boldsymbol{Y}^{\rm eq}(T_b, p_b, \boldsymbol{Y}_u)$:

$$\boldsymbol{\omega}\left(T_b, p_b, \boldsymbol{Y}^{\rm eq}(T_b, p_b, \boldsymbol{Y}_u)\right) = 0\,. \tag{46}$$

The dependence of $\boldsymbol{Y}^{\rm eq}(T_b, p_b, \boldsymbol{Y}_u)$ on $\boldsymbol{Y}_u$ results from the constraint that their detailed *atomic* compositions must be the same. After all, chemistry is nothing but a re-arrangement of atoms (and energy) between molecules. The appropriate mathematical description is

$$\sum_{j=1}^{n_{\rm spec}} \nu_i^j \, \frac{1}{\mathcal{M}_j}\,(Y_{j,b} - Y_{j,u}) = 0 \qquad (i = 1 \ldots n_{\rm atoms})\,, \tag{47}$$

where ν_i^j is the number of atoms of type i in a molecule of species j, and $\mathcal{M}_j$ is the molecular weight of species j.

3.2. CHARACTERISTIC ANALYSIS

We turn next to the question in which way a reactive discontinuity influences its surrounding flow field and in which way it must respond, in turn, to input from outside. Since in most practical applications the Reynolds and Peclet numbers are very large, important insight can be gained by analyzing the inviscid flow equations. Moreover, we are interested here in the behaviour of the flow *surrounding* a reactive front, so that we may restrict our discussion to the case of a reactive discontinuity embedded between the masses of non-reactive burnt and unburnt gases.

Thus we consider the conservation equations

$$\begin{array}{rcrcl} (\rho)_t & + & (\rho u)_x & = & 0 \\ (\rho u)_t & + & (\rho u^2 + \frac{1}{M^2}\,p)_x & = & 0 \\ (\rho e)_t & + & (u[\rho e + p])_x & = & 0. \end{array} \tag{48}$$

with

$$\rho e = \frac{p}{\gamma - 1} + \frac{M^2}{2}\rho u^2\,. \tag{49}$$

Applying the chain rule of differentiation repeatedly and forming a number of linear combinations one may transform these equations to the quasi-linear form

$$\begin{array}{rcrcl} \rho_t & + & u\,\rho_x & + & \rho\,u_x = 0 \\ u_t & + & u\,u_x & + & \frac{1}{M^2}\frac{1}{\rho}\,p_x = 0 \\ p_t & + & u\,p_x & + & \gamma p\,u_x = 0. \end{array} \tag{50}$$

(In fact, the chain rule immediately yields $(50)_1$, subtraction of [$u \times (48)_1$] from $(48)_2$ yields $(50)_2$ and subtraction of [$u \times (48)_2$] from $(48)_3$ yields $(50)_3$.)

Now subtraction of [$(\gamma p/\rho) \times (50)_1$] from $(50)_3$ yields the first compatibility condition of the theory of characteristics:

$$(p_t + up_x) - c^2\,(\rho_t + u\rho_x) = 0 \tag{51}$$

where

$$c = \sqrt{\frac{\gamma p}{\rho}} \tag{52}$$

is the scaled speed of sound. Similarly, by adding and subtracting [$(M\,\rho c)$ $\times$ $(50)_2$] to / from $(50)_3$ one obtains the compatibility conditions

$$\begin{aligned} \left(p_t + (u + \tfrac{1}{M}c)\,p_x\right) \;+\; M\,\rho c\;\left(u_t + (u + \tfrac{1}{M}c)\,u_x\right) \;&=\; 0 \\ \left(p_t + (u - \tfrac{1}{M}c)\,p_x\right) \;-\; M\,\rho c\;\left(u_t + (u - \tfrac{1}{M}c)\,u_x\right) \;&=\; 0\,. \end{aligned} \tag{53}$$

The operators

$$\left(\frac{\partial}{\partial t}\right)_{\rm pp} = \frac{\partial}{\partial t} + u\,\frac{\partial}{\partial x} \qquad \text{and} \qquad \left(\frac{\partial}{\partial t}\right)^{\pm}_{\rm ac} = \frac{\partial}{\partial t} + (u \pm \tfrac{1}{M}c)\,\frac{\partial}{\partial x} \tag{54}$$

are "directional derivatives", describing time derivatives as seen by observers "pp" and "ac" moving with velocities u and $u \pm \frac{1}{M}c$, respectively. The observer motions $x_{\rm pp}(t)$ and $x^{\pm}_{\rm ac}(t)$ thus obey the evolution equations

$$\frac{dx_{\rm pp}}{dt} = u \qquad \text{and} \qquad \frac{dx^{\pm}_{\rm ac}}{dt} = u \pm \tfrac{1}{M}c\,. \tag{55}$$

In other words, $(\partial/\partial t)_{\rm pp}$ indicates temporal variations seen along a particle path, whereas $(\partial/\partial t)^{\pm}_{\rm ac}$ denotes time derivatives seen by an observer moving with an acoustic signal.

The three compatibility conditions from Equations (51) and (53) contain the same information as the original conservation laws (48) or the primitive formulation (50) as long as all required derivatives exist. The key advantage of this "characteristic formulation" is that it explicitly shows how information is transported in time. We will use this insight now to discuss the mathematical features of gas dynamic discontinuities. We consider Figure 3 and ask, what information is available at any given time to determine the two states immediately in front of and behind a discontinuity together with its front propagation speed: For the species mass fractions we have $n_{\rm spec}$ equations from Equations (44) and (47), allowing us to determine the burnt gas composition, once the unburnt composition and the burnt gas pressure

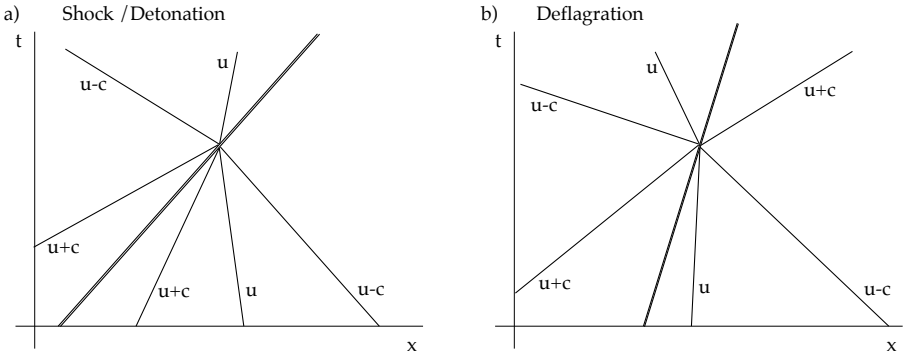

Figure 3. Characteristic diagrams for shocks and detonations (a) and deflagrations (b).

and temperature (or density) are known. (For a non-reactive front, such as a shock wave, these reduce to the condition that the species mass fractions do not change across the front.)

Differentiating the fluxes $\rho Y_i u$ in the species transport equations (2) and neglecting the right hand side expressions one finds compatibility conditions for the species mass fractions in the unburnt gas,

$$\boldsymbol{Y}_t + u\,\boldsymbol{Y}_x = 0\,. \tag{56}$$

These equations state that the species mass fractions do not change along particle paths outside the reaction front. Based on this, one finds the unburnt gas composition in front of a discontinuity at any time t as follows: Track the particle path $dx_{pp}/dt = u$, which arrives at the front at time t, backwards in time until you reach the initial time $t = 0$. The composition found at that location is the same as the unburnt gas composition near the front at the later instance t (cf. Figure 3).

Thus we only need to check whether there is a sufficient number of equations to determine pressures, densities, and velocities in the burnt and unburnt, (p_b, ρ_b, u_b) and (p_u, ρ_u, u_u), plus the front propagation speed D. These are alltogether 7 unknowns.

Consider Figure 3a which shows the sketch of a propagating shock or (overdriven) detonation wave. The number of characteristic curves that *arrive* at the discontinuity from earlier times is 4. Adding the 3 jump conditions from (43), we have 7 equations for the seven unknowns. These turn out to be independent equations, and thus the burnt and unburnt states plus the propagation speed D are completely determined just through the equations of motion, the species transport equations outside the front, the Hugoniot jump conditions, and suitable initial or boundary data or both.

The situation is different for deflagrations as can be seen in Figure 3b. The forward acoustic signal $dx^+_{ac}/dt = u + \frac{1}{M}c$ *emerges from* the dis-

continuity rather than *arriving at it*. Thus the associated compatibility conditions can only be used in determining the further evolution but not to connect the current states near the front to the given initial (and boundary) conditions. One determining equation for (p_b, ρ_b, u_b), (p_u, ρ_u, u_u) and D is missing! The missing relation is a burning velocity eigenvalue, providing an explicit functional relation between the pre- and post-front states and the propagation speed D. The burning rate law is typically given as

$$D = u_u + s(p_u, \rho_u, \boldsymbol{Y}_u) \tag{57}$$

with some explicit function $s(p, \rho, \boldsymbol{Y})$.

That a flame speed law must be provided in order to uniquely determine the propagation of a deflagration wave has a deeper physical reason than just the "number counting game" pursued above. Shock waves as well as detonations are governed by inviscid gas dynamics only. Chemical reactions in detonations are triggered by shock wave compression, and their exremely high, supersonic propagation speed renders the effects of molecular transport irrelevant. Once a shock has sufficiently compressed the gas, temperatures are high enough to lead to auto-ignition, and the reaction heat release sets in. The rate of fuel consumption is determined completely by this compression-ignition-reaction sequence that involves inviscid gas dynamics only.

This is in contrast to the physics of deflagrations. Here, the hot burnt gases preheat the unburnt gas right in front of the flame through heat conduction (or radiation or both) and chemical radicals diffuse out of the reaction zone into the unburnt gas region. Once this process of preheating and chemical preconditioning has lead to sufficient reactivity, combustion takes place and the front propagates. The whole process hinges on heat conduction and species diffusion, both of which are not represented in the characteristic analysis of the inviscid flow equations given above. We conclude that

- The detailed processes within the flame structure crucially influence the flame propagation.

4. Capturing of Shocks and Detonations

4.1. SHOCK CAPTURING SCHEMES FOR COMPRESSIBLE FLOWS

The numerical technology for simulating fully compressible flows has advanced to quite a mature state over the past two decades. Numerous textbooks and fundamental texts elucidate the basic ideas, (LeVeque, 1992), the advanced analysis, (Kröner, 1996; Kröner et al., 1998; Hughes, 1995;

Löhner et al., 1997), and practical applications in combustion (Oran and Boris, 1987). The cited references include finite-volume as well as finite-element approaches. Here, we summarize only the key difficulties associated with compressible flow simulation and sketch some numerical approaches to overcome them.

Weak solutions of non-linear hyperbolic equation systems. The key challenge in the context of compressible flow simulation is to accurately handle non-linear hyperbolic waves and shock formation. Two critical features of such weak solutions must be addressed, namely (i) that shock waves travel at speeds that are determined by the constraints of mass, momentum, and energy conservation, and (ii) that standard central finite difference approximations tend to invoke spurious oscillations next to steep gradients. Such oscillations are particularly critical in the context of reactive flow simulations because they may interact with chemical kinetic models to produce false numerical predictions.

The importance of conservation. The first issue, obtaining the correct weak solutions, was partially resolved by Lax and Wendroff (1960). The authors proved that IF a numerical method converges AND is in conservation form, THEN it converges to weak solutions of the underlying conservation laws. This result determined much of the further developments, in that major research went into the design of automatically conservative numerical methods in which cell averages of the conserved quantities are updated by balancing fluxes across grid-cell interfaces. It should be noticed, though, that deviations from conservation mainly affect simulations for situations with strong shocks (order $O(1)$ pressure changes across). Weakly compressible flows, in which non-linear wave propagation essentially follows the theory of characteristics, can be simulated quite well with non-conservative, high-accuracy methods, see (Hughes, 1995; Geratz et al., 1996; Löhner et al., 1997; Bijl and Wesseling, 1998; Roller et al., 1999).

Regarding the suppression of spurious oscillations, two successful strategies have been developed:

- Non-linear artificial dissipation and
- non-linear upwind techniques.

Non-linear dissipation via flux correction. The most prominent representative of the first group is the the "flux corrected transport" (FCT) family of schemes. The underlying idea is to combine a dissipative first-order accurate numerical method that completely damps oscillations with a scheme of

higher accuracy that may allow the development of oscillations. A non-linear correction scheme is invoked which, depending on local solution features, forces a transition from the high-accuracy scheme to the more dissipative one. These corrections are added only where necessary, so that the overall accuracy is that of the sophisticated scheme in regions of smooth solution, while the damping capabilities of the dissipative scheme are explored next to discontinuities. Fourth- and higher-order accurate versions of these FCT schemes have been proposed and are being used for combustion simulations (Oran and Boris, 1987; Williams et al., 1996).

Non-linear upwind schemes. The second group of schemes, using non-linear upwind techniques, was pioneered by Godunov, see e.g., (Einfeldt, 1988; LeVeque, 1992; Kröner, 1996). A key observation is that the "damping" that occurs near shocks in gas dynamics is restricted to the extremely thin shock transition region, which is of a thickness comparable to merely a few mean free paths of the gas molecules. Hence standard second- or higher-order dissipation is absent and cannot be responsible for the piecewise smooth, non-oscillatory solution behaviour close to physical shocks. The characteristic analysis of section 3.2 shows that oscillations are controlled by the directed transport of information along characteristics (in one space dimension), which terminate when reaching a shock front and whose information is then dissipated instantaneously.

Godunov suggested a numerical approach that would automatically incorporate this non-linear selection of information transport, thereby avoiding the need for artificial viscosity terms. He proposed to compute the fluxes across grid-cell interfaces in a numerical scheme in conservation form by exactly solving local "Riemann problems" (essentially equivalent to the standard shock tube problem, but with generalized initial states). These solutions use the non-linear wave nature of the underlying system to resolve the jumps of state quantities between adjacent grid-cells.

This basic structure proposed by Godunov has been taken up and developed further in various directions, the most established ones being higher-order extensions (the essentially non-oscillatory (ENO)-version of the approach achieves accuracies comparable to those of FCT schemes), and simplifications replacing the Godunov's exact Riemann solutions by approximate ones. The latter are easier to generalize to systems with non-trivial equations of state and are generally more efficient. For further details, see the (Oran and Boris, 1987; LeVeque, 1992; Kröner, 1996) and references therein.

4.2. DETONATION CAPTURING

The mathematical nature of detonation waves is very similar to that of ordinary gas dynamic shocks. Therefore, one expects that the numerical schemes in the conservation form should be able to also "capture" detonation waves. In fact, the basic argument stating that conservative numerical schemes should produce the correct weak solutions if they converge can also be applied to detonations. As a consequence, there is a multitude of applications of FCT schemes or Godunov-type methods to problems of detonation physics, (see the past Combustion Symposia, the Shock Wave Symposia or the ICDERS conferences).

There is one caveat, though, which leads to surprising unphysical effects if overlooked (Colella et al., 1986). In the limit of rapid chemistry, equivalent to under-resolved representation of the detonation reaction zone, numerical schemes can develop numerical solutions that appear to be reasonable at a first glance but are in fact unphysical. The origin is an undesired non-linear interaction between the numerical dissipation resulting from averaging over grid-cells between time steps and the highly non-linear combustion chemistry.

The effect has been studied and analysed in quite some detail by Colella et al. (1986) on the basis of an "operator splitting" technique for the reactive Euler equations. The idea of operator splitting is to (i) decompose the governing equations from (1), (2) into separate equations describing inert flow and chemical reaction progress, and to (ii) construct a numerical method for the full equations by alternatingly solving these separated equations. The input for a "flow step" then is the last output from the "reaction step" and vice versa, see (Strang, 1968).

Suppose we intend to simulate a propagating detonation in a single space dimension for a reactive gas with very fast and very temperature sensitive reactions. The initial data might be set up to match exactly the Rankine-Hugoniot jump conditions as described in (43). Then the first "gasdynamic step" will send a strong shock wave into the first grid cell containing unburnt gases. The resulting gas compression will considerably raise the gas temperature. In the subsequent "reaction step" the temperature sensitive chemistry will be triggered and, due to it being extremely fast, it will completely burn the gas within that grid cell. The result is a front the propagates at a speed of one grid cell per time step essentially regardless of the time increment. Obviously, this will be an unphysical "combustion front" whose origin is an intricate interaction of numerical dissipation and the modelled chemical reactions. Colella et al. (1986) found that this front corresponds to a "weak detonation", which can be observed in nature only under very special conditions, followed by an ordinary gasdynamic shock in the burnt gases.

This problem has been addressed in various ways, partly heuristic, partly theoretically founded, by Colella et al. (1986), Oran and Boris (1987), LeVeque and Yee (1990), Pember (1993), and Berkenbosch et al. (1998). In the last of the cited references an approach has been suggested that is particularly simple and easy to implement, while it avoids some pitfalls of alternative methods. The proposed scheme makes use of the following two observations:

1. The burnt gas temperature behind a weak detonation *decreases* with *increasing* front speed.
2. The slowest weak detonation has the same end state as the slowest strong (regular, physically correct) detonation. This limiting case is called a "Chapman-Jouguet-Detonation".
3. The burnt gas state behind the weak detonation is reached directly through a reaction step.

The idea of the fake detonation remedy is to introduce an artificial chemistry switching temperature in such a way that chemical reactions are suppressed for temperatures lower than this threshold, while they proceed according to the original chemical kinetic scheme for higher temperatures. By choosing the switching temperature to match a Chapman-Jouguet-detonation's burnt gas temperature *minus* the temperature increment from a "reaction step" that completely burns the original mixture, one can reliably suppress the undesired fake weak detonation waves.

5. Deflagration Waves

Chemical reactions are typically very fast once ignited. The available fuel is quickly burned and reactions are concentrated in narrow regions with characteristic thicknesses of the order of fractions of a millimetre. A systematic derivation, showing how fast reaction ($\mathrm{Da} \gg 1$), and inefficient molecular transport ($\mathrm{Re}, \mathrm{Pe} \gg 1$) conspire to lead to thin laminar flames with finite propagation speeds is given in (Majda and Sethian, 1985). Similar interactions of chemical energy conversion and (turbulent) transport governs the propagation of turbulent deflagrations. There are two very different alternative approaches towards numerical representation of deflagrations, namely

1. detailed modelling of the inner flame structure, and
2. flame front tracking.

5.1. RESOLVED TURBULENT FLAME STRUCTURES

By this first approach one implements numerical representations of both the overall reaction and (turbulent) transport mechanisms that are active within the flame region. For correct results, equal emphasis must be given to either of these subprocesses. An excellent mean reaction rate model would, for example, be useless unless combined with an equally sophisticated effective turbulent transport scheme. In addition the "full-resolution approach" requires sufficient spatial and temporal numerical resolution of the flame region in order to achieve the desired accuracy in representing the reaction-transport interplay.

In summary, the advantages of this approach are:

- All important physical sub-mechanisms within a turbulent flame zone as well as their interactions can be incorporated.
- The mathematical structure of the most popular turbulent combustion models is similar to a combination of standard non-reactive turbulent flow models and the laminar reactive Navier-Stokes equations. Thus available reactive flow solvers can be employed more or less "out of the box" for turbulent combustion simulations.

The disadvantages are that

- A detailed representation of the turbulent flame brush structure leads to minimum spatial resolution requirements that can become overwhelming for large-scale, industrial-size systems. This issue may enforce the use of dynamically adaptive grids, with all the added complexity.
- The second advantage cited above only holds when the turbulent combustion model excludes certain non-standard effects, such as countergradient turbulent transport (Bray et al., 1982; Bray et al., 1989). If such effects are important, adequate numerical techniques must be implemented.

There is currently no widespread consensus regarding the proper mathematical structure of a turbulent combustion model. Therefore, little general advice can be given regarding the numerical techniques that should be employed or developed in order to cope with the arising complexities. The reader should consult (Warnatz et al., 1996; Vervisch et al., 1999; Peters, 2000) for an extensive collection of related material!

5.2. FLAME FRONT TRACKING

Flame front tracking approaches avoid the necessity of modelling the complex phenomena within a "flame brush", (Chorin, 1980; Smiljanovski and

Klein, 1994; Hilditch and Colella, 1995; Smiljanovski et al., 1997; Fedkiw et al., 1998). They represent a deflagration as a reactive discontinuity and obtain a closed equation system by supplying an explicit burning rate law as a function of the unburnt gas thermodynamic, composition, and turbulence state.

The advantages of this approach are:

- that it explicitly controls the net mass burning rate without relying on subtle interactions between submodels of net turbulent reaction rates and effective turbulent transport, and
- that it allows much coarser spatial and temporal resolution, because it avoids a detailed representation of the internal flame structure.

Its major disadvantage is that

- one must supply effective turbulent flame speed functions and effective jump conditions, which can be derived from scratch only in particular regimes of (turbulent) combustion.

From a practical point of view, however, supplying measured effective turbulent burning velocities might be easier to achieve experimentally than distinguishing detailed subprocesses within a flame brush by localized measurements.

Flame front tracking requires the numerical representation of the flame geometry and its evolution (→ Section 5.2.1) *and* of the coupling between front and surrounding flow via the Rankine-Hugoniot conditions (43) or generalizations of these for highly unsteady flames (→ Section 5.2.2).

5.2.1. *The level set or "G-equation" approach*
As discussed above, premixed flames propagate relative to the unburnt gas at the local burning velocity s. For a two-dimensional setting, the situation is sketched in Figure 4. The propagation of points on a flame surface is determined by the superposition of convection by the unburnt gas flow and this self-propagation in the direction normal to the front

$$d\,\boldsymbol{x}_f/dt = \boldsymbol{v}_u + s\boldsymbol{n} =: \boldsymbol{D}. \tag{58}$$

Here $\boldsymbol{n}$ is a unit normal vector on the front pointing towards the unburnt gas region. The level set or "G-equation" approach introduces a scalar field $G(\boldsymbol{x}, t)$ whose iso-surfaces

$$G(\boldsymbol{x}, t) = G_0 \tag{59}$$

are identified with flame fronts. Then

$$\boldsymbol{n} = -\left.\frac{\nabla G}{|\nabla G|}\right|_{G=G_0}. \tag{60}$$

The choice of G_0 is arbitrary but fixed for a single combustion event. The flame surface(s) $G = G_0$ naturally decompose the flow domain into unburnt gas ($G < G_0$) and burnt gas regions ($G > G_0$). Differentiating (59) with respect to time and using (58) one finds

$$\frac{\partial G}{\partial t} + \frac{d\boldsymbol{x}_f}{dt} \cdot \nabla G = \frac{\partial G}{\partial t} + \boldsymbol{D} \cdot \nabla G = 0\,, \tag{61}$$

the G-equation.

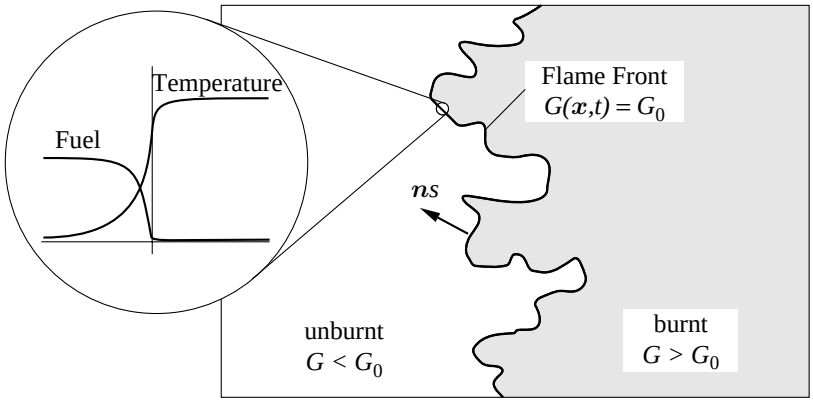

Figure 4. Schematic representation of premixed flame front propagation

The key physical ingredients of the level set approach are the burning velocity law determining s as a function of thermo-chemical and flow conditions and some local features of the flame geometry. It is important to notice that s is defined as the relative velocity between points on the front and the unburnt gas immediately *in front* of it. The relative velocity s_b between the burnt gas and the front differs from s because of the thermal gas expansion within the flame front and the associated jump of the normal velocity. Because of mass conservation the mass flux density normal to the front does not change across the discontinuity and the burnt gas relative speed is easily computed as

$$\rho s = (\rho s)_b = \rho_u s \quad \Rightarrow \quad s_b = \frac{\rho_u}{\rho_b} s\,. \tag{62}$$

Although both the flow velocity and the relative speed between flow field and front change across the flame, their sum, namely the vector $\boldsymbol{D}$ appearing in (61), does not! This observation will be important in the subsequent construction of a numerical method.

Figure 5 shows the temporal evolution of an initially sinusoidally distorted front according to (61), with $s \equiv const.$ and with the unburnt gas at rest. The front motion then follows Huygens' principle and one quickly

observes the formation of sharp cusps on the front. Laminar flame theory, (Matalon and Matkowsky, 1982; Clavin, 1985), as well as modern theories of turbulent premixed combustion, (Libby and Williams, 1994; Peters, 1992; Peters, 2000), yield modified, curvature dependent burning velocity laws of the type

$$s = s^0 - s^0 \mathcal{L}\kappa + \mathcal{L}\boldsymbol{n} \cdot \nabla \boldsymbol{v} \cdot \boldsymbol{n} \quad \text{where} \quad \kappa = \nabla \cdot \boldsymbol{n} \tag{63}$$

is the mean front curvature. The second and third terms describe the net effect of the (turbulent) diffusive processes (second term) and by outer straining of the flame by the surrounding flow field (third term). In detail, s^0 is the burning velocity of a plain, unstrained flame, $\mathcal{L}$ is an effective Markstein length, and κ is the local mean front curvature. As indicated in

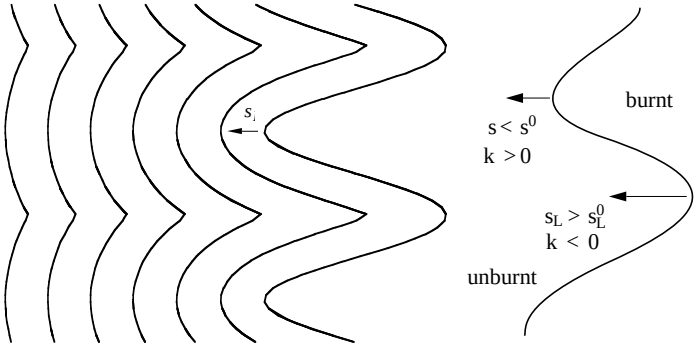

Figure 5. Flame propagation according to (61) for constant burning velocity s; schematic for the influence of curvature.

Figure 5 the curvature is defined to be positive when the front is convex w.r.t. the unburnt gas and vice versa. For positive Markstein numbers the curvature term thus prohibits the formation of sharp cusps on the flame front.

Determination of level sets away from the tracked front. There is one important issue that needs to be accounted for when dealing with "real" flames within which substantial chemical heat is released. The propagation (61) is valid at the flame front only, since only at the front is the burning velocity s properly defined. Thus one needs to introduce additional constraints determining the time evolution of the scalar G away from the tracked interface. One option, proposed in Reference (Sussman et al., 1994), is to require the level set scalar to be a signed distance function away from the front. This is equivalent to requiring that

$$|\nabla G| = 1 \tag{64}$$

and the additional requirement that G be negative in the unburnt and positive in the burnt gas region. For numerical techniques to enforce the distance function property, see (Sussman et al., 1994; Fedkiw et al., 1998; Adalsteinsson and Sethian, 1999; Strain, 1999).

5.2.2. *Flame-flow coupling*
Having adopted the level set approach to describe the evolution of the flame front geometry, one must next describe the mutual interactions between the tracked front and the surrounding flow. From (58) and (61) it is clear how the unburnt gas flow affects the flame motion: The flame propagation velocity consists of (i) passive advection by the unburnt gas velocity and (ii) of self-propagation induced by combustion. The unburnt gas conditions influence this latter part through explicit burning velocity laws such as (63).

The front, in turn, influences the surrounding flow by enforcing the flame discontinuity jump conditions (43) for the flow variables at the flame location $G(\boldsymbol{x}, t) = G_0$. Various methods have been developed in recent years to realize this coupling in the context of finite-volume methods, (Chern and Colella, 1987; Bourlioux and Majda, 1992; LeVeque and Shyue, 1996; Smiljanovski et al., 1997; Terhoeven, 1998; Fedkiw et al., 1999; Klein, 1999). These schemes mainly differ in their degree of complexity and detail and in their applicability to compressible and incompressible flows.

Chern and Colella (Chern and Colella, 1987), Bourlioux and Majda (Bourlioux and Majda, 1992), and LeVeque and Shyue (LeVeque and Shyue, 1996) consider compressible flows and treat the moving front surface as part of their time dependent numerical grid. For each of the subcells generated when a front intersects a grid-cell of the underlying computational mesh a complete conservative flux update is performed. The CFL type time-step restrictions associated with updating small subcells are overcome by distributing excess accumulations of the conserved quantities among the neighbouring grid-cells. The schemes differ in how this is done in detail, but they all follow this common pattern.

The method described in Reference (Smiljanovski et al., 1997), which is also designed for compressible flows, compromises on the former schemes in that only *complete grid-cells* are updated by flux balances. The flame-generated subcells are used only in an "in-cell reconstruction step", which recovers burnt and unburnt gas conditions from the cell averages using a suitable set of recovery equations (see the appendix). The consequence is that, while the scheme *does* conserve mass, momentum, and energy between grid-cells and globally, it is *not* conservative with respect to these subcells. The method therefore does not automatically conserve mass, momentum, and energy between the pre- and post-front regions. For flame fronts, this just amounts to numerical truncation errors affecting the net burning rate

and is not critical. However, in tracking a passive non-reactive fluid interface, such as the surface of a water droplet in air, this scheme would not conserve the droplet mass. An associated improvement is work in progress (Schneider et al., 1999).

Terhoeven (1998) and Klein (1999), to our knowledge, are the first to propose a flame front tracking scheme for zero Mach number flows in the finite-volume context (see, however, also Helenbrook et al. (1999)). The key ideas are the same as those in Reference (Smiljanovski et al., 1997), but there are important modifications that become indispensable in the limit of small and zero Mach numbers. The key difficulty has been discussed earlier in Section 2. The second-order pressure p_2 in a low Mach number pressure expansion is responsible for flow accelerations. Within the flame discontinuity there is an order $O(1)$ density change and an associated flow acceleration. This can be accomplished only through a pressure discontinuity. The consequence is that the second-order pressure must satisfy a Poisson equation with a singular source term that ensures the appropriate pressure jump across the flame surface. For more detail the reader may wish to consult the original references.

Fedkiw et al. (1999) again consider compressibe flows, but go one step further in simplifying the approach. By compromising on conservation also for the complete "mixed cells", they are able to design a numerical method that is very attractive because of its simplicity and nearly dimension-independent formulation.

A sample result obtained using the capturing/tracking hybrid scheme from Reference (Smiljanovski et al., 1997) is described in Figs. 6 and 7. The RUT test h11 has been reproduced using a two-dimensional approximation, a standard $k-\epsilon$ turbulence model, and Damköhler's law to represent the effective turbulent burning velocity as

$$s_T = s_L + u' \qquad \text{where} \qquad u' = \sqrt{2k} \tag{65}$$

with k from the $k-\epsilon$ model data in the unburnt gas immediately in front of the flame. The coloured density contours show the propagation of the sharp flame surface in time, and the second figure shows a comparison of space-time diagrams of the flame tip location as taken from experiment and computation. It turns out that the initial phase is slightly misrepresented, in that the computed flame acceleration is too slow. Yet as soon as the first obstacle is reached, the experimental and computed flame locations agree convincingly well.

It is remarkable that this scheme, which was developed to handle fully compressible flows spends about 90 % of its computation time to propagate the flame from initiation as a circle to the first obstacle. The reason is that

at this early stage the flow is still very slow, with Mach numbers of order 10^{-3}.

Notice also that the considerable deviation of observation and simulation during the initial phase of the process can be explained: The simulation is two-dimensional and starts with a circle, whereas the real event is fully three-dimensional and starts with a small, almost spherical flame kernel. It is clear that the initial evolutions are not comparable.

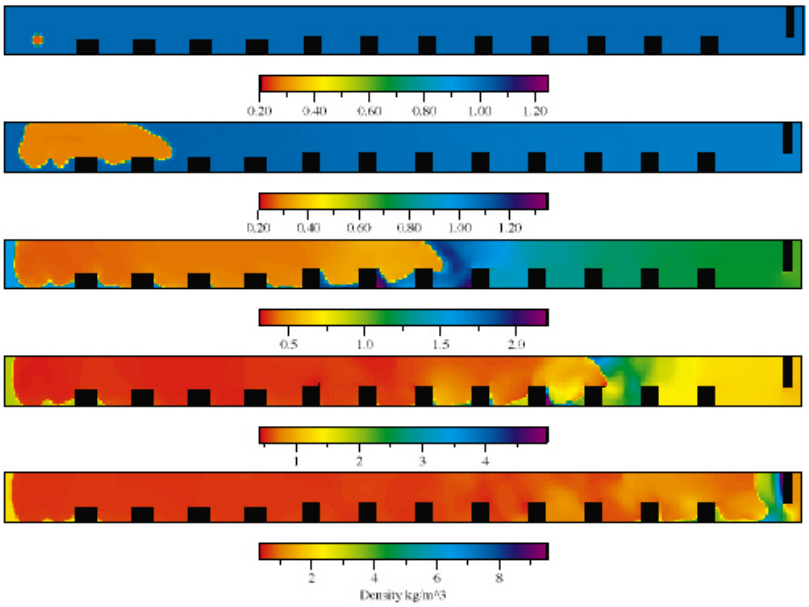

Figure 6. Sequence of density contours as computed in a two-dimensional model for RUT test h11 using the flame front capturing/tracking hybrid scheme from Reference

6. The Deflagration-to-Detonation Transition (DDT)

This section provides a brief, qualitative discussion of known or hypothesized mechanisms for flame acceleration and the transition to detonation. DDT is one of the most demanding challenges in numerical combustion due to the wide range of different physical effects that are involved and need to be modelled. Numerical codes that can cope with these problems are currently under development within various research groups.

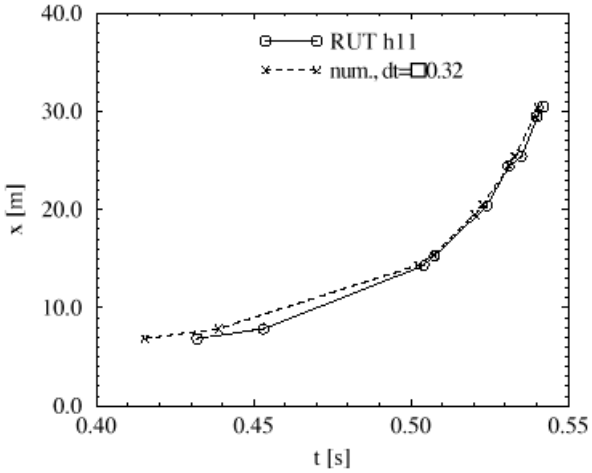

Figure 7. Comparison of the time history of flame propagation in the test case from Figure 6

6.1. FLAME ACCELERATION: SMALL SCALE TURBULENT WRINKLING VERSUS GLOBAL FLAME AREA INCREASE

Consider the example discussed in the context of figures 6, 7. There are two distinct mechanisms that could be responsible for the observed dramatic flame acceleration:

Turbulent Flame Front Wrinkling: The initially laminar thin flame encounters an unburnt gas flow field with increasing levels of turbulence. The turbulent fluctuations, through the $\boldsymbol{v}_u$-part of the flame propagation velocity $\boldsymbol{D}$ in (58), will distort the flame surface, wrinkle and corrugate it, and will thus lead to a local effective flame area increase, see (Damköhler, 1940) for Damköhler's original discussion, or (Peters, 2000).

Global Flame Area Increase: At the same time, the thermal gas expansion associated with combustion generates a global flow field along the channel. There is a distinct asymmetry, as the flow is confined in all directions, except one. As a result, the flame will be stretched out extensively along the channel, and this leads to a global (rather than local) flame area increase.

Experimentation with a quasi-onedimensional toy model in (Breitung et al., 1999b) has shown that the first mechanism alone has a much less dramatic influence than the latter. In fact it was observed that with this mechanism alone a flame would quickly settle into a quasi-stationary propagation regime with an effective speed that is higher than the laminar burning

velocity, but definitely subsonic. The second mechanism, in contrast, led to continous, unbounded flame acceleration consistent with the simulations discussed above.

6.2. THE BIRTH OF A DETONATION

Suppose now that a turbulent flame is accelerating to speeds that become comparable with the speed of sound through the mechanisms described above. The next issue then is the initiation of sufficiently strong shock waves that can directly ignite fresh gas without the mediation of turbulent and/or molecular transport. Three different mechanisms are currently deemed possible or that have even been observed within experiments and/or direct numerical simulations, see (Breitung et al., 1999b; Breitung et al., 1999a).

Shock-Induced Ignition and Shock Wave Generation (DDT Mode A): The accelerating flame produces a strong precursor flow due to the thermal gas exansion that is induced by combustion. When the turbulent flame reaches effective propagation speeds comparable with the speed of sound, the precursor flow becomes fully compressible and is associated with strong shocks. As such shocks are reflected off the surface of obstacles or are even focused in room corners or other convex wall configurations, pressure and temperature overshoots occur that are sufficient to locally ignite the gas. Fully established detonation waves can emerge from such explosion centers (Ref. (Breitung et al., 1999b)). Note that these processes take place at locations that are clearly separated from the zone of turbulent combustion.

Quenching, Reignition, and Shock Wave Generation (DDT Mode B): The second mechanism, in contrast, is intimately related to processes that take place within the turbulent flame brush. The most well-established theories of turbulent combustion agree in presuming that reactions take place within thin, connected reaction fronts, even when considerable turbulence intensities are encountered (Peters, 2000). It is known, however, that such reactive fronts can endure only a limited amount of strain by the surrounding flow field. Thus for a given reactive mixture there is a level of turbulence at which the most intense turbulent fluctuations manage to locally quench these reaction fronts. At these locations, one suddenly has hot burnt and cold unburnt gases in close contact without a mechanism for keeping them separate. Turbulent mixing then quickly generates smoothed distributions of species concentrations and temperatures. Within this region, the reactants are now heated by the hot reaction products and they will undergo reignition. When autoigniting gas pockets are sufficiently energetic, they

generate shock waves that may lead to shock-reaction coupling and to the establishment of detonations.

Acoustics – Ignition Resonances in Pre-Shocked Gases (DDT Mode C): It is commonly accepted that "transverse waves", which are families of weaker, obliquely propagating shocks trailing the main detonation shock, are essential for the self-sustaining of detonation waves. Experiments by J.H.S. Lee (see a discussion in (Breitung et al., 1999a)) have in fact shown that detonations in obstacle-loaden shock tubes can be quenched by preparing the tube walls so that they absorbe acoustic fluctuations. Consider now a high-speed turbulent deflagration and the precursor shock that it generates. Between the precursor shock and the deflagration front there is pre-conditioned fresh gas that is driven closer and closer towards auto-ignition. At the same time, multiple transverse shocks will occur due to reflection of the leading shock off obstacles and other geometrical non-uniformities. It is believed that an agglomeration of such transverse waves on top of the pre-conditioned gas can lead the coupling between the precursor and the reaction front necessary for the establishment of a detonation wave.

7. Summary

This paper has outlined some of the key difficulties associated with the numerical simulation of premixed combustion processes. Emphasis has been given to the singular limit regimes of low Mach number flow, and rapid chemical reactions. It has been shown how an analytical understanding of these limit regimes aids in constructing appropriate numerical methods. Thus we have discussed in section 2 the relation between flow solvers for compressible and incompressible flows, and we have shown how one may bridge the gap between these seemingly incompatible families of methods by exploiting the insight gained through low Mach number asymptotics. Section 3 summarized some mathematical features of reactive (and non-reactive) discontinuities, thereby laying the ground for the discussion of flow solvers for detonation and deflagration waves in sections 4 and 5. It turned out that detonation waves can be represented robustly using more or less standard numerical compressible flow solvers after a judicious modification of the numerical representation of reaction progress. In contrast, the mathematical properties of deflagration waves require more involved numerical techniques, such as level set methods for flame front tracking. Section 6 provided a mostly qualitative description of the current knowledge on processes of Deflagration-to-Detonation Transition. These processes involve, within a single overall phenomenon, all the various difficulties described

earlier in the paper. Currently, the construction of numerical methods that function with uniform accuracy and efficiency across this wide range of singular limit regimes remains a major challenge. The author is convinced that success will come from a close cooperation of scientists from the disciplines of combustion theory, and applied and numerical mathematics. The inherently turbulent nature of most combustion processes will in addition require thorough validation by comparison of computational results with measurements from carefully chosen sets of experiments.

References

Adalsteinsson, D. and J. A. Sethian: 1999, 'The Fast Construction of Extension Velocities in Level Set Methods'. *Journal of Computational Physics* **148**, 2–22.

Almgren, A., J. Bell, P. Colella, L. Howell, and M. Welcome: 1996, 'A Conservative Adaptive Projection Method for the Variable Density Incompressible Navier-Stokes Equations'. *LBNL Preprint* **39075 UC-405**.

Bell, J. B. and D. L. Marcus: 1992, 'A Second-Order Projection Method for Variable-Density Flows'. *Journal of Computational Physics* **101**, 334–348.

Berger, M. J. and P. Colella: 1989, 'Local Adaptive Mesh Refinement for Shock Hydrodynamics'. *Journal of Computational Physics* **82**, 67–84.

Berkenbosch, A. C., R. Kaaschieter, and R. Klein: 1998, 'Detonation Capturing for Stiff Combustion Chemistry'. *Combustion Theory and Modelling* **2**.

Bijl, H. and P. A. Wesseling: 1998, 'Unified Method for Computing Incompressible and Compressible Flows in Boundary-Fitted Coordinates'. *Journal of Computational Physics* **141**, 153173.

Bourlioux, A. and A. J. Majda: 1992, 'Theoretical and Numerical Structure for Two-Dimensional Unstable Detonations'. *Combustion and Flame* **90**, 211–229.

Bray, K. N. C., M. Champion, and P. A. Libby: 1989, 'The Interaction between Turbulence and Chemistry in Premixed Turbulent Flames'. In: R. Borghi and S. Murphy (eds.): *Turbulent Reacting Flows*.

Bray, K. N. C., J. Moss, and P. A. Libby: 1982, 'Turbulent Transport in Premixed Turbulent Flames'. In: J. Zierep and H. Oertel (eds.): *Convective Transport and Instability Phenomena*.

Breitung, W., C. Chan, S. B. Dorofeev, A. Eder, B. E. Gelfand, M. Heitsch, R. Klein, A. Malliakos, J. E. Shepherd, E. Studer, and P. Thibault: 1999a, 'SOAR on Flame Acceleration and DDT in Nuclear Reactor Safety'. to be published by the OECD.

Breitung, W., I. Coe, H. Grönig, L. He, R. Klein, H. Olivier, W. Rehm, E. Studer, and B. Wang: 1999b, *Models and Criteria for Prediction of Deflagration-to-Detonation Transition (DDT) in Hydrogen-Air-Steam Systems under Severe Accident Conditions*, Projekt FI4S-CT96-0025 - Final Report. European Commission, Brussels.

Chern, I. and P. Colella: 1987, 'A Conservative Front Tracking Method for Hyperbolic Conservation Laws'. UCRL-97200, Lawrence Livermore National Laboratory.

Chorin, A. J.: 1967, 'A Numerical Method for Solving Incompressible Viscous Flow Problems'. *Journal of Computational Physics* **2**, 12–26.

Chorin, A. J.: 1968, 'Numerical Solution of the Navier-Stokes Equations'. *Mathematics of Computation* **22**, 745–762.

Chorin, A. J.: 1969, 'On the Convergence of Discrete Approximations to the Navier-Stokes Equations'. *Mathematics of Computation* **23**, 341–353.

Chorin, A. J.: 1980, 'Flame Advection and Propagation Algorithms'. *Journal of Computational Physics* **35**, 1–11.

Clavin, P.: 1985, 'Dynamic Behavior of Premixed Flame Fronts in Laminar and Turbulent Flows'. *Progress in Energy and Combustion Science* **11**, 1–59.

Colella, P., A. Majda, and V. Roytburd: 1986, 'Theoretical and Numerical Structure for Reacting Shock Waves'. *SIAM Journal of Scientific and Statistical Computing* **7**, 1059–1080.

Damköhler, G.: 1940, 'Der Einfluss der Turbulenz auf die Flammengeschwindigkeit in Gasgemischen [The Influence of Turbulence on Flame Velocities in Gas Mixtures]'. *Zeitschrift für Elektochemie und angewandte Physikalische Chemie* **46**, 601–626. See also NACA Technical Memorandum 1112, 1947.

Einfeldt, B.: 1988, 'On Godunov-Type Methods for Gas Dynamics'. *SIAM Journal of Numerical Analysis* **25**, 294–318.

Fedkiw, R., T. Aslam, and S. Xu: 1998, 'The Ghost Fluid Method for Deflagration and Detonation Discontinuities'. submitted to Journal of Computational Physics.

Fedkiw, R. P., T. Aslam, and S. Xu: 1999, 'The Ghost Fluid Method for Deflagration and Detonation Discontinuities'. *Journal of Computational Physics* **xx**, to appear.

Fletcher, C. A. J.: 1988, *Computational Techniques for Fluid-Dynamics—Fundamental and General Techniques*, Vol. 2. Springer Verlag, New York.

Geratz, K., R. Klein, C.-D. Munz, and S. Roller: 1996, 'Multiple Pressure Variable (MPV) Approach for Low Mach Number Flows Based on Asymptotic Analysis'. In: E. H. Hirschel (ed.): *Flow Simulation with High-Performance Computers II. DFG Priority Research Programme Results*, Notes on Numerical Fluid Mechanics, Vol. 53. Vieweg Verlag, Braunschweig.

Geratz, K. J.: 1998, 'Erweiterung eines Godunov-Typ-Verfahrens für mehrdimensionale kompressible Strömungen auf die Fälle kleiner und verschwindender Machzahl'. Ph.D. thesis, RWTH Aachen.

Gresho, P. M., R. L. Sani, and M. Engelman: 1991, *Incompressible Flow and the Finite Element Method*. John Wiley & Sons, New York.

Haldenwang, P., J. Daou, B. Denet, and C. Nicoli: 1998, 'Low Mach Number Combustion Modelling for Droplet and Spray'. presented at 5th Intl. Conference on Numerical Combustion, SIAM, York, UK, March 30 - April 1, 1998.

Helenbrook, B. T., L. Martinelli, and C. K. Law: 1999, 'A Numerical Method for Solving Incompressible Flow Problems with a Surface of Discontinuity'. *Journal of Computational Physics* **148**, 366–396.

Hilditch, J. and P. Colella: 1995, 'Front Tracking Method for Compressible Flames in one Dimension'. *SIAM Journal of Scientific Computing* **16**, 755–772.

Hughes, T. J. R.: 1995, 'Multiscale Phenomena: Greens Functions, the Dirichlet-to-Neumann Formulation, Subgrid Scale Models, Bubbles and the Origins of Stabilized Methods'. *Computer Methods in Applied Mechanics and Engineering* **l27**, 387–401.

Issa, R. I.: 1986, 'Solution of the Implicitly Discretised Fluid Flow Equations by Operator-Splitting'. *Journal of Computational Physics* **62**, 40–65.

Karki, K. C. and S. V. Patankar: 1989, 'Pressure Based Calculation Procedure for Viscous Flows at all Speeds in Arbitrary Configurations'. *AIAA Journal* **27**, 1167–1174.

Kim, J. and P. Moin: 1985, 'Application of a Fractional Step Method to Incompressible Navier-Stokes Equations'. *Journal of Computational Physics* **59**, 308–323.

Klein, R.: 1995, 'Semi-Implicit Extension of a Godunov-Type Scheme Based on Low Mach Number Asymptotics I: One-Dimensional Flow'. *Journal of Computational Physics* **121**, 213–237.

Klein, R.: 1999, 'Numerics in Combustion'. In: L. Vervisch, D. Veynante, and D. Olivari (eds.): *Introduction to Turbulent Combustion*.

Klein, R. and N. Peters: 1988, 'Cumulative Effects of Weak Pressure Waves During the Induction Period of a Thermal Explosion in a Closed Cylinder'. *Journal of Fluid Mechanics* **187**, 197–230.

Knio, O. M. and A. S. Worlikar: 1996, 'Numerical Simulation of a Thermo-Acoustic Refrigerator: I Unsteady adiabatic flow around the stack'. *J. Comput. Physics* **127**, 424.

Knio, O. M., A. S. Worlikar, and R. Klein: 1998, 'Numerical Simulation of a Thermo-Acoustic Refrigerator: II Stratified flow around the stack'. *J. Comput. Physics* **144**, 299–324.

Knio, O. M., A. S. Worlikar, and R. Klein: 1999, 'Numerical Study of the Effective Impedance of a Thermo-Acoustic Stack'. *Acoustica* **85**, 480–494.

Kröner, D. (ed.): 1996, *Numerical Schemes for Conservation Laws*. Wiley and Teubner, Stuttgart, Leipzig.

Kröner, D., M. Ohlberger, and C. Rhode (eds.): 1998, *An Introduction to Recent Developments in Theory and Numerics for Conservation Laws*, Lecture Notes in Computional Science and Engineering, Vol. 5. Springer, Berlin, Heidelberg, New York.

Lai, M., J. B. Bell, and P. Colella: 1993, 'A Projection Method for Combustion in the Zero Mach Number Limit'. Technical Report 93-3369, AIAA paper.

Lang, J.: 1998, 'Adaptive Incompressible Flow Computations with Linearly Implicit Time Discretization and Stabilized Finite Elements'. In: K. Papailiou, D. Tsahalis, J. Periaux, C. Hirsch, and M. Pandolfi (eds.): *Computational Fluid Dynamics '98*. John Wiley & Sons, New York.

Lax, P. D. and B. Wendroff: 1960, 'Systems of Conservation Laws'. *Communications in Pure and Applied Mathematics* **13**, 568–582.

LeVeque, R. and H. Yee: 1990, 'A Study of Numerical Methods for Hyperbolic Conservation Laws with Stiff Source Terms'. *Journal of Computational Physics* **86**, 187–210.

LeVeque, R. J.: 1992, *Numerical Methods for Conservation Laws*. Birkhäuser Verlag, Zürich, Schweiz. IBSN 0-521-43009-7.

LeVeque, R. J. and K.-M. Shyue: 1996, 'Two-Dimensional Front Tracking Based on High Resolution Wave Propagation Methods'. *Journal of Computational Physics* **123**, 35–368.

Libby, P. A. and F. Williams: 1994, *Turbulent Reacting Flows*. London, UK: Academic Press.

Löhner, R., K. Morgan, J. Peraire, and M. Vahdati: 1997, 'Finite Element Flux Corrected Transport (FEM-FCT) for the Euler and Navier-Stokes Equations'. *International Journal for Numerical Methods in Fluids* **7**, 1093–1109.

Majda, A. and J. Sethian: 1985, 'The Derivation and Numerical Solution of the Equations for Zero Mach Number Combustion'. *Combustion Science and Technology* **42**, 185–205.

Matalon, M. and B. J. Matkowsky: 1982, 'Flames as Gasdynamic Discontinuities'. *Journal of Fluid Mechanics* **124**, 239–259.

Oran, E. and J. Boris: 1987, *Numerical Simulation of Reactive Flow*. Elsevier Science Publ., New York.

Patankar, S. V.: 1980, *Numerical Heat Transfer and Fluid Flow*. Hemisphere Publishing Corporation.

Pember, R. B.: 1993, 'Numerical Methods for Hyperbolic Conservation Laws with Stiff Relaxation I. Spurious Solutions'. *SIAM Journal of Applied Mathematics* **53**, 1293–1330.

Pember, R. B., P. Colella, L. H. Howell, A. S. Almgren, J. B. Bell, K. C. Kaufman, W. A. Fiveland, and J. P. Jessee: 1996, 'The Modeling of a Laboratory Natural Gas-Fired Furnace with a Higher-Order Projection Method for Unsteady Combustion'. *LBNL Preprint* **LBNL-38800**.

Peters, N.: 1992, 'A Spectral Closure for Premixed Turbulent Combustion in the Flamelet Regime'. *Journal of Fluid Mechanics* **242**, 611–629.

Peters, N.: 2000, *Turbulent Combustion*. Cambridge University Press, Cambridge, UK.

Rannacher, R.: 1992, 'On Chorin's Projection Method for the Incompressible Navier-Stokes Equations'. In: J. G. Heywood (ed.): *The Navier-Stokes Equations II—Theory and Numerical Methods*. pp. 167–183.

Rhie, C. M.: 1989, 'Pressure-Based Navier-Stokes Solver Using the Multigrid Method'. *AIAA Journal* **27**, 1017–1018.

Roller, S., C.-D. Munz, K. Geratz, and R. Klein: 1999, 'The Extension of Incompressible Flow Solvers to the Weakly Compressible Regime'. *Theoretical and Numerical Fluid Dynamics* p. submitted for publication.

Schneider, T., N. Botta, R. Klein, and K. J. Geratz: 1999, 'Extension of Finite Volume Compressible Flow Solvers to Multi-Dimensional, Variable Density Zero Mach Number Flows'. *Journal of Computational Physics* **155**, 248–286.

Sesterhenn, J., B. Müller, and H. Thomann: 1992, 'Computation of Compressible Low Mach Number Flow'. *Computational Fluid Dynamics* **2**, 829–833.

Shyy, W.: 1994, 'Elements of Pressure-Based Computational Algorithms for Complex Fluid Flow and Heat Transfer'. *Advances in Heat Transfer* **24**, 191–275.

Smiljanovski, V. and R. Klein: 1994, 'Flame Front Tracking via In-Cell Reconstruction'. In: J. G. et al. (ed.): *5th International Conference on Hyperbolic Systems*. Stony Brook.

Smiljanovski, V., V. Moser, and R. Klein: 1997, 'A Capturing-Tracking Hybrid Scheme for Deflagration Discontinuities'. *Journal of Combustion Theory and Modelling* **2**(1), 183–215.

Strain, J.: 1999, 'Fast Tree-Based Redistancing for Level Set Computations'. *Journal of Computational Physics* **152**, 664–686.

Strang, G.: 1968, 'On the Construction and Comparison of Difference Schemes'. *SIAM Journal of Numerical Analysis* pp. 506–517.

Sussman, M., P. Smereka, and S. Osher: 1994, 'A Level Set Approach for Computing Solutions to Incompressible Two-Phase Flow'. *Journal of Computational Physics* **114**, 146–159.

Teng, Z. H., A. J. Chorin, and T. P. Liu: 1982, 'Riemann Problems for Reacting Gas, with Application to Transition'. *SIAM Journal of Applied Mathematics* **42**(5).

Terhoeven, P.: 1998, 'Ein numerisches Verfahren zur Berechnung von Flammenfronten bei kleiner Mach-Zahl [A Numerical Method for Flame Front Tracking at Low Mach Numbers]'. Ph.D. thesis, RWTH Aachen.

van Kan, J.: 1986, 'A Second-Order Accurate Pressure-Correction Scheme for Viscous incompressible flow'. *SIAM Journal of Scientific and Statistical Computing* **7**, 870–891.

Vervisch, L., D. Veynante, and D. Olivari (eds.): 1999, *Introduction to Turbulent Combustion*. The von Karman Institute, Rhode St. Genese, Belgium.

Warnatz, J., U. Maas, and R. W. Dibble: 1996, *Combustion*. Springer Verlag, New York, Heidelberg, 1. edition.

Williams, D. N., L. Bauwens, and E. S. Oran: 1996, 'Detailed Structure and Propagation of Three-Dimensional Detonations'. In: *26th Symposium (International) on Combustion*. pp. 649–657.